Solubility and Modeling of Sodium Aluminosilicate in NaOH−NaAl(OH)(4) Solutions and Its Application to Desilication

ARTICLE *in* INDUSTRIAL & ENGINEERING CHEMISTRY RESEARCH · NOVEMBER 2012

Impact Factor: 2.59 · DOI: 10.1021/ie301590r

2 AUTHORS:

Zeng Lanmu
Chinese Academy of Sciences
5 PUBLICATIONS **7** CITATIONS

SEE PROFILE

Zhibao Li
Chinese Academy of Sciences
67 PUBLICATIONS **604** CITATIONS

SEE PROFILE

I&EC research
Industrial & Engineering Chemistry Research

Article

pubs.acs.org/IECR

Solubility and Modeling of Sodium Aluminosilicate in NaOH−$NaAl(OH)_4$ Solutions and Its Application to Desilication

Lanmu Zeng and Zhibao Li*

Key Laboratory of Green Process and Engineering, National Engineering Laboratory for Hydrometallurgical Cleaner Production Technology, Institute of Process Engineering, Chinese Academy of Sciences, Beijing 100190, P. R. China

ABSTRACT: The solubility of sodium aluminosilicate (sodalite), a major desilication product (DSP) in the Bayer process, in NaOH and NaOH−$NaAl(OH)_4$ solutions was determined and modeled at temperatures from 303.2 to 348.2 K. Sodium aluminosilicate was synthesized in a batch crystallizer and the effect of temperature, solution concentrations, and aging time was investigated. Solubility was found to increase with increasing NaOH concentration while the solubility sharply decreases with the addition of $Al(OH)_3$, reaches a minimum at about 0.8 mol·L^{-1}, and then increases. A mixed-solvent electrolyte (MSE) model for the solubility of sodalite was developed with the help of the OLI platform via regression to obtain the model parameters. In addition, the desilication kinetics of NaOH−$NaAl(OH)_4$ solutions by using sodalite as seeds was studied experimentally and modeled with the aid of a second order kinetic model. The activation energy of desilication over the temperature range 323.2−363.2 K was found to be 92 ± 14 kJ·mol^{-1}. Under the optimal operation conditions, 80% silica was removed after 2 h.

1. INTRODUCTION

The majority of world alumina production is manufactured from bauxite by the Bayer process.[1] Bauxite is primarily composed of one or more aluminum hydroxide minerals such as gibbsite, boehmite and diaspore, and also contains other compounds such as silica, iron, titanium and impurities in minor amount.[2] In the Bayer process, bauxite is attacked by caustic liquor at high temperature to dissolve the aluminum hydroxide as well as silica minerals, such as kaolinite and quartz. The dissolved silica in the Bayer liquor reacts with the sodium aluminate to form sodium aluminosilicate which has low solubility. Silica is a highly undesirable impurity in the Bayer liquor for two reasons: when the precipitation of sodium aluminosilicate occurs at the stage of gibbsite crystallization, it will contaminate the product; and in the evaporation stage of the spent liquor, it tends to form scale on the surface of the heat exchangers and thus increases the operation costs.[3−5]

Low-grade diasporic bauxite ores with low ratios of alumina to silica (A/S:4−6) cannot be processed economically by the conventional Bayer process.[6−8] Therefore, several processes such as sintering, floating, and lime Bayer process have been developed to deal with high silica diasporic bauxite.[9] However, these processes suffer from one or more disadvantages. For example, the hurdle of implementation for the lime Bayer process is that it is not sufficiently effective for processing low-grade bauxite ores with A/S < 5.[10] Recently, Ma et al.[11] in our laboratory proposed a new process including a predesilication stage where the reactive silica is dissolved and stabilized in the concentrated NaOH−$NaAl(OH)_4$ solution. After solid/liquid separation, the A/S of bauxite can be enhanced to 10, suitable for the conventional Bayer process, while the filtrate with high silica up to 10 g/L is desilicated by the addition of CaO to achieve the acceptable silica level before entering the crystallization stage. But this desilication method yields a significant loss of alumina and extra CaO cost.[12] On the other hand, the high silica level in the filtrate gives an opportunity via seeded crystallization to precipitate a "pure" sodium aluminosilicate as DSP.[13] By doing this, 'pure' sodium aluminosilicate can be obtained as a saleable byproduct, for example as an anticaking agent,[14] while reducing the loss of alumina and CaO usage.

For a better understanding of the desilication reaction with sodium aluminosilicate seed, it is necessary to know the solubility and crystal growth kinetics of sodium aluminosilicate. Furthermore, knowledge of the solubility of sodium aluminosilicate can help to understand the silica precipitation and the scaling process in the crystallization and evaporation stages of the Bayer process. Sodium aluminosilicate is a large family containing phases such as amorphous sodium aluminosilicate, zeolites, sodalite, and cancrinite.[15] The most commonly found phase at moderate temperature, such as in the desilication process, is sodalite.[16] The solubility of sodium aluminosilicate has been studied intensively over the years and is summarized in Table 1. However, there exist many inconsistencies in these published solubilities. For example, the solubility of zeolite A measured by Ejaz et al.[17] is greater than that of Addai-Mensah et al.[18] Oku and Yamda[19] and other researchers[20] found that the solubility is temperature independent while increasing solubility with increased temperature was reported in other studies.[5,17,18] The solubility of sodalite in concentrated NaOH−$NaAl(OH)_4$ solutions with the low temperature range (<363.2 K), has not been reported.

The polymerization of silicon species in alkaline solutions creates a tremendously complicated system. Successful modeling the solubility of sodalite in NaOH and NaOH−$NaAl(OH)_4$ solutions requires reasonable simplifications based on the operating conditions in the Bayer process. Gasteiger et al.[21] supposed orthosilic acid ($HSiO_4^{3-}$) to be the predominant silicon species by use of the Pitzer model to account for the activity coefficients, while Park et al.[22] assumed that SiO_3^{2-} is the most

Received: June 17, 2012
Revised: October 8, 2012
Accepted: October 29, 2012
Published: October 29, 2012

   dx.doi.org/10.1021/ie301590r | *Ind. Eng. Chem. Res.* 2012, 51, 15193−15206

Table 1. Reported Solubility of Sodium Aluminosilicate in Literature

authors	experimental conditions		temp (K)	phase
	C(NaOH) mol·L^{-1}	C(Al(OH)$_3$) mol·L^{-1}		
Breuer et al. 1963	1.0−4.8	0.1−3.4	343.2−523.2	sodalite and zeolite A
Ni et al. 1964	4.0−14.3	0.2−6.5	363.2	undetermined
Čizmek et al. 1991	1.00−2.00		338.2−353.2	zeolite A
Kali Zheng et al. 1998	4.53	1.62	363.2−433.2	sodalite
Barnes et al 1999	3.47−5.42	1.39−2.23	363.2−433.2	sodalite
Ejaz et al. 1999	3.02−4.39		303.2−353.2	zeolite A and amorphous
Addai-Mensah et al. 2004	3.00−6.00		303.2−403.2	zeolite A and amorphous

important silicon species. However, the aluminosilicate polyanions, which are confirmed by Raman spectra and may be the main silicon species in the Bayer liquor,[23] has not been taken adequately into consideration in previous studies.

In the present investigation, the sodalite, which is stable in the desilication stage in the new process, was obtained by batch reactions, and the effect of temperature, aging time, and other factors was investigated. The solubility of sodalite synthesized under the optimal conditions was determined in 0−8.5 mol·L^{-1} NaOH solutions and mixed NaOH−NaAl(OH)$_4$ solutions containing 3.95−9.85 mol·L^{-1} NaOH at 303.2−348.2 K by the isothermal dissolution method. On the basis of the speciation of the Na_2O−Al_2O_3−SiO_2−H_2O system, a chemical model for predicting the solubility of sodalite was established. In addition, the desilication kinetics of NaOH−NaAl(OH)$_4$ solutions by use of sodalite seeds was studied at fixed Na_2O and Al_2O_3 concentrations.

2. EXPERIMENTAL SECTION

2.1. Experimental Materials. Analytical grade NaOH, Al(OH)$_3$, and $Na_2SiO_3·9H_2O$ were supplied by Xilong Chemical Co. Ltd. with purities 98.0%, 99.4%, and 98.5%, respectively. All solutions used in this study were prepared by dissolving analytical grade chemicals directly without further purification. Deionized water with specific conductivity of 0.1 μS·cm^{-1} was used.

2.2. Preparation of NaOH−NaAl(OH)$_4$ Solutions. To prepare a NaOH−NaAl(OH)$_4$ stock solution containing the required content of alkali and alumina, Al(OH)$_3$, NaOH, and deionized water were mixed at room temperature until all NaOH was dissolved. This mixture was then heated to a boiling point with stirring until an optically clear solution was formed. When cooled, water was added to make up a 1 L liquid. The stock solution was stored in a sealed 1 L polypropylene bottle placed in an air bath at 350.2 K until use.

2.3. Synthesis of Sodium Aluminosilicate. A 1 L glass tank reactor equipped with a central two-blade Teflon impeller, that provides constant agitation, was used for synthesizing sodium aluminosilicate (Figure 1). The reactor was heated by the circulating oil from a thermostat bath to control temperature to within ±0.5 K. The synthesis was conducted by preheating prepared NaOH−NaAl(OH)$_4$ solution to a desired temperature. Then an equal volume of sodium metasilicate solution was added at a given rate by a peristaltic pump, while stirring at 300 rpm. When the addition was completed, stirring continued for 0−3 h. The entire mixture was then filtered under reduced pressure. The resultant filter cake was resuspended in a 1 L polypropylene beaker using about 800 mL of deionized water or 300 mL of ethanol before being refiltered. This washing/refiltering was repeated 2 times using deionized water and 1 time using ethanol. The washed filter cake was finally dried in an oven at 328.2 K for 10 h.

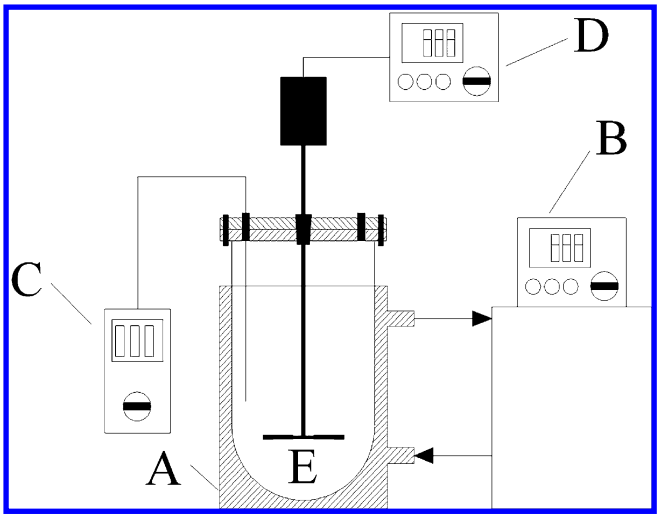

Figure 1. Schematic of the sodium aluminosilicate synthesis apparatus: (A) heating jacket; (B) oil circulator; (C) thermometer; (D) impeller controller; (E) impeller.

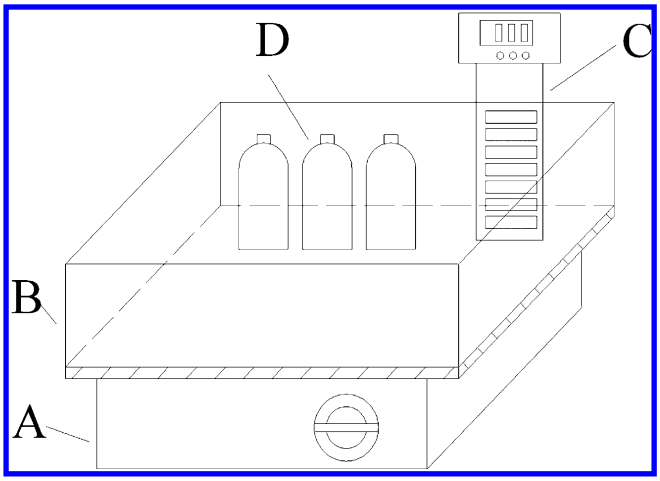

Figure 2. Schematic of the solubility measurement apparatus: (A) magnetic stirring plate; (B) water bath; (C) heating circulator; (D) bottle with cap.

2.4. Measurement of Solubility. The solubility determination can be done either by the dissolution method or the precipitation method.[24] The dissolution method was adopted in this work since Breuer et al.[25] found that the solubility equilibrium was not reached after 600 h at 343.2 K by the precipitation method.

The solubility was measured inside a 250 mL Teflon bottle. A 4 g portion of prepared sodalite solid and 200 mL stock NaOH−NaAl(OH)$_4$ solution were added to the bottle. The bottles were then immersed in an electrically heated, thermostatically

dx.doi.org/10.1021/ie301590r | Ind. Eng. Chem. Res. 2012, 51, 15193−15206

controlled water bath with constant magnetic stirring (Figure 2). The temperature was kept constant to within ±0.1 K. To reach equilibrium, the solution is continuously stirred for 48 h, and later, the solution is allowed to settle for at least 1 h before sampling. Samples of the saturated liquid phase were after collected using plastic syringes equipped with nylon filters (0.22 μm). The filtrate was placed in a preweighed 25 mL volumetric flask and immediately weighed (±0.1 mg) to measure the density of the saturated solution. Finally, the SiO_2 concentration of the saturated solution was analyzed. CO_2 can be adsorbed from the air into alkaline solutions and is also frequently present as an impurity in solid NaOH. To minimize the effect of CO_3^{2-} on the solubility, N_2 gas was used to remove the absorbed CO_2 in all liquids before use. Furthermore, the bottles were tightly capped by using rubber stoppers to avoid CO_2 uptake during the solubility determination.

2.5. Desilication with Sodalite Seeds. Desilication experiments were performed in the above-mentioned glass tank reactor. A solution containing 250 g·L^{-1} NaOH, 286.75 g·L^{-1} $Al(OH)_3$ (187.5 g·L^{-1} Al_2O_3), and 10 g·L^{-1} SiO_2 was placed in the reactor operating at 300 rpm agitation rate and at a constant temperature. Once the temperature was attained, 19.2 or 38.4 g of prepared sodalite seed were immediately introduced into the reactor. During desilication, slurry samples were periodically withdrawn and immediately filtered through nylon filters (0.22 μm) for analysis of the SiO_2 concentration.

2.6. Chemical Analysis and Characterization. The SiO_2 concentration in the solution was analyzed by ammonium molybdate spectrophotometry using a UNICOUV-2000 ultraviolet−visible spectrophotometer. Solid products were examined using power X-ray diffraction (XRD) and scanning electron microscopy (SEM, JEOL-JSM-6700F). Powder XRD (X'Pert PRO MPD, PANalytical, Almelo, The Netherlands) patterns were recorded on a diffractometer (using Cu Kα radiation) operating at 40 kV/40 mA. A scan rate of 0.02 deg/s was applied over the 2θ angle range of 5°−90°. X-ray fluorescence (XRF) was used to determine the chemical composition of the sodium aluminosilicate samples.

3. MODELING METHODOLOGY

3.1. Speciation of Aluminum and Silicon in Alkaline Aqueous Solution. The speciation of aluminum and silicon species plays an important role in the chemical modeling for the $Na_2O-Al_2O_3-SiO_2-H_2O$ system. The speciation of aluminum in aqueous solutions over a wide range of pH has been studied by several investigators.[26−28] Normally, the $Al(OH)_4^-$ ion is the predominant species at pH greater than 10.[27] Unfortunately, the speciation of silicon species in an aqueous alkali solution is much more complicated because a striking variety of oligomeric silicon anions may exist in the alkaline solution. As a general rule, the larger silicate oligomers are favored by greater silicon concentration and reduced alkalinity and temperature.[29] For example, Provis et al. found that there are many oligomeric silicon anions in a sodium silicate solution with $SiO_2/Na_2O = 2$ and $H_2O/Na_2O = 11$ at room temperature, while monomeric silicate anions are the major silicon species at $SiO_2/Na_2O = 0.25$ and $H_2O/Na_2O = 11$.[30] In the present study, it is reasonable to assume that only monomeric silicate anions, namely $H_2SiO_4^{2-}$ and $HSiO_3^-$, may exist under typical operation conditions of the Bayer process due to the low silicon concentration (Na_2O/SiO_2 ratio >100) and high alkalinity (Na_2O > 100 g·L^{-1}).

In addition to polymerization, silicon species may complex with $Al(OH)_4^-$ to form aluminosilicate polyanions.[15,23] Jolivet et al. pointed out that these aluminosilicate species never contain Al−O−Al bonds because aluminate cannot autocondense.[15] So in the typical Bayer liquor with aluminate to silicate ratio greater than 100, aluminosilicate anion (Al/Si ratio equal to 1) should predominant over aluminosilicate polyanions. As suggested by Gout et al.,[23] the formation of the aluminosilicate anion is independent of OH^- concentration and could be written as $AlSiO_3(OH)_4^{3-}$.

3.2. Chemical Equilibria. For the $Na_2O-Al_2O_3-SiO_2-H_2O$ system, the mixed solvent electrolyte (MSE) model[31−33] embedded in the OLI platform[34] was selected as the modeling tool because its chemistry includes suitable dissociation reactions of complex silicon species, such as monomeric $HSiO_3^-$ and $H_2SiO_4^{2-}$ as well as a polyanionic $AlSiO_3(OH)_4^{3-}$. The main dissolution/dissociation reactions of the $Na_2O-Al_2O_3-SiO_2-H_2O$ system could be written as

$$Na_8(AlSiO_4)_6(OH)_2\cdot 2H_2O(\text{sodalite}) + 10H_2O + 10OH^- = 8Na^+ + 6Al(OH)_4^- + 6H_2SiO_4^{2-} \quad (1)$$

$$Al(OH)_3(\text{gibbsite}) + OH^- = Al(OH)_4^- \quad (2)$$

$$HSiO_3^- + OH^- = H_2SiO_4^{2-} \quad (3)$$

$$AlSiO_3(OH)_4^{3-} + H_2O = H_2SiO_4^{2-} + Al(OH)_4^- \quad (4)$$

For solids, namely sodalite and gibbsite, the solubility product constants are

$$K_{SP}(\text{sodalite}) = \frac{(m_{Na^+}\gamma_{Na^+})^8 (m_{Al(OH)_4^-}\gamma_{Al(OH)_4^-})^6 (m_{H_2SiO_4^{2-}}\gamma_{H_2SiO_4^{2-}})^6}{(m_{OH^-}\gamma_{OH^-})^{10}(a_w)^{10}} \quad (5)$$

$$K_{SP}(\text{gibbsite}) = (m_{Al(OH)_4^-}\gamma_{Al(OH)_4^-})/(m_{OH^-}\gamma_{OH^-}) \quad (6)$$

For soluble species the thermodynamic equilibrium constants for reactions 3 and 4 are given by

$$K(HSiO_3^-) = \frac{m_{H_2SiO_4^{2-}}\gamma_{H_2SiO_4^{2-}}}{(m_{HSiO_3^-}\gamma_{HSiO_3^-})(m_{OH^-}\gamma_{OH^-})} \quad (7)$$

$$K(AlSiO_3(OH)_4^{3-}) = \frac{(m_{H_2SiO_4^{2-}}\gamma_{H_2SiO_4^{2-}})(m_{Al(OH)_4^-}\gamma_{Al(OH)_4^-})}{(m_{AlSiO_3(OH)_4^{3-}}\gamma_{AlSiO_3(OH)_4^{3-}})(a_w)} \quad (8)$$

where K is the thermodynamic equilibrium constant; m is the the molality concentration of relevant species (mol·kg^{-1} H_2O); and γ is the activity coefficient of the relevant species.

The estimation of sodalite solubility requires knowledge of the thermodynamic equilibrium constants, the activity coefficient of relevant ions, and the activity of water.

3.3. Thermodynamic Framework. The thermodynamic equilibrium constants in the MSE model are calculated using the following equation:

$$K = \exp\left(-\frac{\Delta_R \bar{G}^\circ}{RT}\right) \quad (9)$$

$\Delta_R\bar{G}^\circ$ is the partial molal, standard-state Gibbs free energy of reaction, R is the gas constant (8.314 J·mol^{-1}·K^{-1}) and T is the temperature (Kelvin). To obtain the equilibrium constants, the standard-state chemical potentials of the products and reactants must be known. For solids, the standard-state chemical potentials are calculated from the standard-state Gibbs free energy of formation ($\Delta_f\bar{G}^\circ$), entropy (S°) and heat capacity (C_p°) according

dx.doi.org/10.1021/ie301590r | Ind. Eng. Chem. Res. 2012, 51, 15193−15206

to standard thermodynamic relationships. For aqueous species, the HKF model, developed by Tanger and Helgeson,[35] is used to evaluate the standard-state chemical potentials.

While thermodynamic equilibrium constants are used to calculate the chemical equilibriums, the nonideality of an electrolyte solution is represented by the excess Gibbs free energy. In the MSE model, the excess Gibbs free energy is constructed as follows:

$$\frac{G^{ex}}{RT} = \frac{G^{ex}_{LR}}{RT} + \frac{G^{ex}_{MR}}{RT} + \frac{G^{ex}_{SR}}{RT} \tag{10}$$

where G^{ex}_{LR} represents the contribution of long-range electrostatic interactions expressed by the Piter−Debye−Hückel equation; G^{ex}_{SR} is the short-range contribution resulting from molecule/molecule, molecule/ion, and ion/ion interactions calculated by the UNIQUAC model; and an additional middle-range term G^{ex}_{MR} accounts for ionic interactions that are not included in the long-range term. G^{ex}_{MR} is calculated from a symmetrical second-virial coefficient-type expression:

$$\frac{G^{ex}_{MR}}{RT} = -\left(\sum_i n_i\right)\sum_i\sum_j x_i x_j B_{ij}(I_x) \tag{11}$$

where x is the mole fraction of the species, I_x represents the ionic strength, B_{ij} is a binary interaction parameter between the species i and j (ion or molecule) and $B_{ij}(I_x) = B_{ji}(I_x)$, $B_{ii}(I_x) = B_{ij}(I_x) = 0$. B_{ij} is a function of ionic strength represented by the following empirical expression:

$$B_{ij}(I_x) = b_{ij} + c_{ij}\exp(-\sqrt{I_x + 0.01}) \tag{12}$$

where b_{ij} and c_{ij} are adjustable parameters. In general, the parameters b_{ij} and c_{ij} are calculated as functions of temperature as

$$b_{ij} = \mathrm{BMD0} + \mathrm{BMD1}T + \mathrm{BMD2}/T + \mathrm{BMD3}T^2 + \mathrm{BMD4}\ln T \tag{13}$$

Table 2. Synthesis Recipe for Sodium Aluminosilicate

sample	reaction temp (K)	initial NaOH ($mol\cdot L^{-1}$)	initial $Al(OH)_3$ ($mol\cdot L^{-1}$)	initial SiO_2 ($mol\cdot L^{-1}$)	titration speed (mL/min)	aging time (min)
1-a	303.2	12	3	3	5	20
1-b	333.2	12	3	3	5	20
1-c	363.2	12	3	3	5	20
2-a	333.2	8	2	2	5	20
2-b	333.2	12	4	4	5	20
2-c	333.2	12	3	3	10	20
2-d	333.2	12	3	3	1.67	20
3-a	333.2	12	3	3	5	0
3-b	333.2	12	3	3	5	180
3-c	363.2	12	3	3	5	180

$$c_{ij} = \mathrm{CMD0} + \mathrm{CMD1}T + \mathrm{CMD2}/T + \mathrm{CMD3}T^2 + \mathrm{CMD4}\ln T \tag{14}$$

BMD0, BMD1, CMD0, and CMD1, etc. are the interaction parameters.

In practice, the middle-range parameters are used to account for ion−ion and ion−neutral molecule interaction and the short-range parameters are used to represent neutral−neutral interaction. The middle-range parameters are mainly considered in this work because these are most important for electrolyte solutions.

3.4. Desilication Modeling Framework. The kinetics of precipitation may be complicated due to the influence of surrounding ions.[36] For the precipitation of silica from NaOH−$NaAl(OH)_4$ solutions, we found that a simple second order kinetic model as developed by Barnes et al. could be employed.[37] In the model, the driving force for desilication is expressed as a function of relative supersaturation of SiO_2:

$$\sigma = (C - C_{eq})/C \tag{15}$$

where C ($mol\cdot L^{-1}$) is the SiO_2 concentration at any time and C_{eq} ($mol\cdot L^{-1}$) is the equilibrium concentration.

For isothermal batch desilication, the decreasing SiO_2 concentration may be caused by nucleation and crystal growth mechanisms. The kinetics of the two mechanisms may be quantified as

$$-\frac{d\sigma}{dt} = k_n\sigma^n + Ak_g\sigma^2 \tag{16}$$

where k_n is the rate constant for nucleation (h^{-1}); n is the order of the nucleation reaction; A is the total surface area of crystals (m^2); and k_g is the growth rate constant ($h^{-1}\cdot m^{-2}$).

In the seeded desilication reactions, as many nuclei existed, the influence of nucleation was omitted, and surface crystal growth was assumed as the only reason for the decreasing SiO_2 concentration. Equation 16 simply reduces to the form below:

$$-\frac{d\sigma}{dt} = Ak_g\sigma^2 \tag{17}$$

With the assumption that the total surface area remains unchanged, the concentration of SiO_2 as a function of time was obtained by integrating eq 17:

$$C = \frac{C_0 - C_{eq}}{1 + k_g At(C_0 - C_{eq})/C_{eq}} + C_{eq} \tag{18}$$

where C_0 is the initial SiO_2 concentration ($mol\cdot L^{-1}$), and t is the batch desilication time (h).

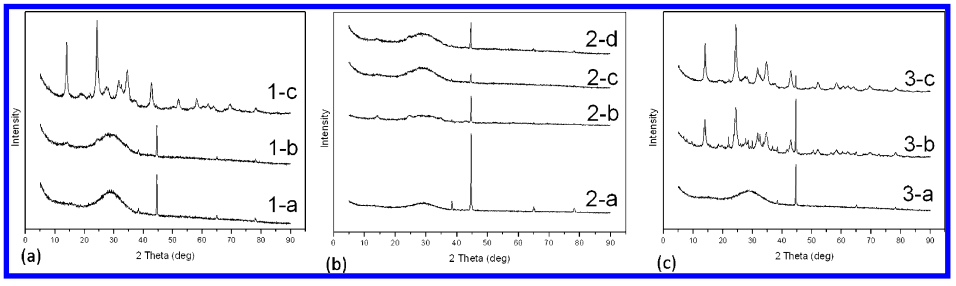

Figure 3. XRD patterns of sodium aluminosilicate prepared using different conditions.

dx.doi.org/10.1021/ie301590r | Ind. Eng. Chem. Res. 2012, 51, 15193−15206

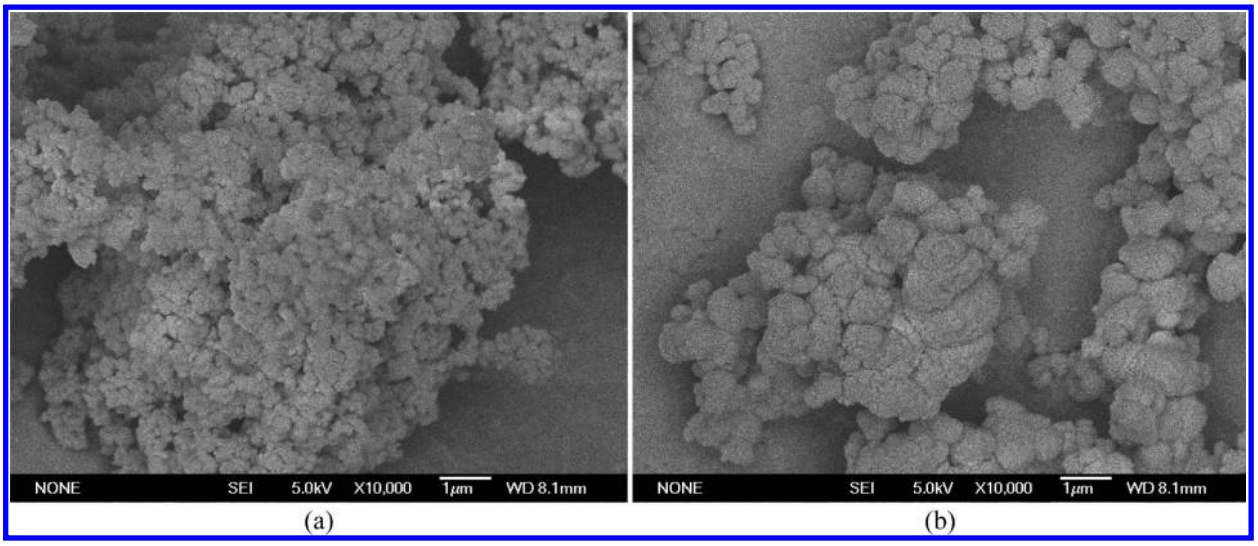

Figure 4. SEM morphologies of amorphous sodium aluminosilicate and sodalite prepared at 363.2 K. (amorphous type on the left, sodalite on the right).

4. RESULTS AND DISCUSSION

4.1. Characterization of Synthesized Sodium Aluminosilicate. The synthesis recipe for sodium aluminosilicate is listed in Table 2, and Figure 3 displays the effect of temperature, initial concentration, titration speed, and aging time on the crystallization of sodium aluminosilicate. In detail, Figure 3a shows that sodalite was obtained when the reaction temperature increased from 333.2 to 363.2 K. As can be seen in Figure 3b, sodium aluminosilicate pecipitated at 333.2 K was still amorphous with variation of the initial concentration and titration speed. Figure 3c indicates that amorphous sodium aluminosilicate (Figure 4a) transformed to sodalite (Figure 4b) at the longer aging time of 3 h. The structural formula of the sodalite sample 3-c $(Na_{7.26}(Al_6Si_{6.12}O_{24})(OH)_{1.68}(H_2O)_{2.91})$ determined by XRF was similar to that of the Na_8-1 sodalite sample $(Na_{7.60}(Al_{5.96}Si_{6.04}O_{24})(OH)_{1.64}(H_2O)_{3.00})$ synthesized by Moloy et al.[38]

4.2. Solubility of Sodium Aluminosilicate in NaOH and NaOH−NaAl(OH)$_4$ Solutions. The measured solubility of sodalite in pure NaOH and mixed NaOH−$NaAl(OH)_4$ solutions is shown in Tables 3 and 4 and Figures 5−9. The results shown in Figure 5 indicate that the solubility of sodalite in NaOH solutions increased with increasing NaOH concentration. As can be seen in Figure 6, the solubility decreased in a nonlinear manner with the addition of $Al(OH)_3$ to fixed 3.95 mol·L^{-1} NaOH solutions. Figures 7 to 9 show that the solubility of sodium aluminosilicate in NaOH−$NaAl(OH)_4$ solutions containing 6.17−9.85 mol·L^{-1} NaOH sharply decreased with the addition of $Al(OH)_3$, reached a minimum at about 0.8 mol·kg^{-1}, and then increased with further increasing $Al(OH)_3$ concentration. The solubility in NaOH and NaOH−$NaAl(OH)_4$ solutions remained almost the same value when the temperature was varied indicating that the effect of temperature on the solubility was negligible. After solubility measurements, XRD characterization of the equilibrated solids, as shown in Figure 10, proves that sodalite was stable in both NaOH or NaOH−$NaAl(OH)_4$ solutions for 48 h.

In addition, literature solubilities of sodium aluminosilicate are displayed in Figures 5 and 6 for comparison. The solubility of sodalite determined in the present work in pure NaOH solutions agreed very well with the solubility of zeolite A measured by Čizmek et al.,[20] but is greater than the solubility of amorphous sodium aluminosilicate and smaller than the solubility of zeolite A obtained by Ejaz et al.[17] (Figure 5). Amorphous sodium aluminosilicate is a thermodynamically unstable phase, thus should have a greater solubility than the thermodynamically stable phase. Figure 6 shows that the solubility results of the present work in NaOH−$NaAl(OH)_4$ solutions was greater than those of Breuer et al.[25] It is worth noting that there was 0.4 mol·L^{-1} Na_2CO_3 in the saturated solution in the determination by Breuer et al., which could be the reason for the decreased solubility.[4] The solubility of zeolite A measured by Čizmek et al., as displayed in Figure 5, is independent of temperature. However, the

Table 3. Solubility of Sodalite in NaOH Solutions

density, g/mL	NaOH, mol·L^{-1}	SiO_2, mol·L^{-1}	NaOH, mol·kg^{-1}	SiO_2, mol·kg^{-1}
		T = 303.2 K		
1.040	1.046	1.07×10^{-2}	1.048	1.07×10^{-2}
1.090	2.615	2.24×10^{-2}	2.654	2.28×10^{-2}
1.143	4.140	3.35×10^{-2}	4.235	3.45×10^{-2}
1.197	5.748	4.12×10^{-2}	5.943	4.30×10^{-2}
1.243	7.167	4.79×10^{-2}	7.493	5.07×10^{-2}
1.286	8.635	5.11×10^{-2}	9.184	5.51×10^{-2}
		T = 318.2 K		
1.046	1.033	1.13×10^{-2}	1.028	1.13×10^{-2}
1.103	2.627	2.31×10^{-2}	2.632	2.33×10^{-2}
1.154	4.258	3.24×10^{-2}	4.330	3.32×10^{-2}
1.205	5.617	4.21×10^{-2}	5.728	4.34×10^{-2}
1.252	7.110	4.81×10^{-2}	7.352	5.03×10^{-2}
1.295	8.556	5.36×10^{-2}	8.982	5.70×10^{-2}
		T = 333.2 K		
1.037	1.037	1.27×10^{-2}	1.041	1.27×10^{-2}
1.095	2.627	2.33×10^{-2}	2.653	2.36×10^{-2}
1.147	4.282	3.34×10^{-2}	4.390	3.45×10^{-2}
1.201	5.636	4.11×10^{-2}	5.780	4.26×10^{-2}
1.251	7.142	4.72×10^{-2}	7.400	4.95×10^{-2}
1.288	8.530	5.47×10^{-2}	9.008	5.86×10^{-2}
		T = 348.2 K		
1.040	1.044	1.33×10^{-2}	1.047	1.33×10^{-2}
1.090	2.623	2.33×10^{-2}	2.663	2.38×10^{-2}
1.143	4.091	3.20×10^{-2}	4.177	3.30×10^{-2}
1.197	5.652	4.06×10^{-2}	5.822	4.22×10^{-2}
1.243	7.219	4.84×10^{-2}	7.563	5.13×10^{-2}
1.286	8.478	5.38×10^{-2}	8.958	5.76×10^{-2}

dx.doi.org/10.1021/ie301590r | Ind. Eng. Chem. Res. 2012, 51, 15193−15206

Table 4. Solubility of Sodalite in NaOH−NaAl(OH)$_4$ Solutions

density, g/mL	$Al(OH)_3$, mol·L^{-1}	SiO_2, mol·L^{-1}	NaOH, mol·kg^{-1}	$Al(OH)_3$, mol·kg^{-1}	SiO_2, mol·kg^{-1}
		NaOH = 3.95 mol·L^{-1}, T = 303.2 K			
1.149	0.0000	3.176×10^{-2}	3.978	0.000	3.218×10^{-2}
1.151	0.0641	1.375×10^{-2}	3.992	0.065	1.395×10^{-2}
1.152	0.1282	8.728×10^{-3}	4.006	0.130	8.877×10^{-3}
1.154	0.1923	6.781×10^{-3}	4.020	0.196	6.919×10^{-3}
1.155	0.2564	5.900×10^{-3}	4.034	0.262	6.040×10^{-3}
1.157	0.3205	5.194×10^{-3}	4.049	0.329	5.335×10^{-3}
1.159	0.3846	4.699×10^{-3}	4.063	0.396	4.843×10^{-3}
1.160	0.4487	4.405×10^{-3}	4.077	0.463	4.556×10^{-3}
		NaOH = 3.95 mol·L^{-1}, T = 318.2 K			
1.150	0.0000	3.176×10^{-2}	3.978	0.000	3.215×10^{-2}
1.158	0.0641	1.403×10^{-2}	3.992	0.065	1.413×10^{-2}
1.156	0.1282	8.952×10^{-3}	4.006	0.130	9.078×10^{-3}
1.163	0.1923	6.935×10^{-3}	4.020	0.196	7.019×10^{-3}
1.161	0.2564	5.774×10^{-3}	4.034	0.262	5.881×10^{-3}
1.167	0.3205	5.234×10^{-3}	4.049	0.329	5.331×10^{-3}
1.163	0.3846	4.802×10^{-3}	4.063	0.396	4.933×10^{-3}
1.151	0.4487	4.147×10^{-3}	4.077	0.463	4.323×10^{-3}
1.164	0.5128	4.537×10^{-3}	4.092	0.531	4.699×10^{-3}
1.174	0.5769	4.603×10^{-3}	4.106	0.600	4.753×10^{-3}
1.171	0.6410	4.653×10^{-3}	4.121	0.669	4.837×10^{-3}
1.179	0.7051	4.620×10^{-3}	4.135	0.738	4.797×10^{-3}
		NaOH = 3.95 mol·L^{-1}, T = 333.2 K			
1.148	0.0000	3.095×10^{-2}	3.978	0.000	3.139×10^{-2}
1.153	0.0641	1.406×10^{-2}	3.992	0.065	1.423×10^{-2}
1.154	0.1282	9.118×10^{-3}	4.006	0.130	9.258×10^{-3}
1.149	0.1923	6.977×10^{-3}	4.020	0.196	7.149×10^{-3}
1.158	0.2564	5.931×10^{-3}	4.034	0.262	6.060×10^{-3}
1.155	0.3205	5.466×10^{-3}	4.049	0.329	5.623×10^{-3}
1.156	0.3846	4.977×10^{-3}	4.063	0.396	5.141×10^{-3}
1.146	0.4487	4.354×10^{-3}	4.077	0.463	4.558×10^{-3}
1.167	0.5128	4.628×10^{-3}	4.092	0.531	4.784×10^{-3}
1.166	0.5769	4.670×10^{-3}	4.106	0.600	4.851×10^{-3}
1.163	0.6410	4.628×10^{-3}	4.121	0.669	4.848×10^{-3}
1.170	0.7051	4.637×10^{-3}	4.135	0.738	4.851×10^{-3}
1.176	0.8333	4.869×10^{-3}	4.165	0.879	5.115×10^{-3}
		NaOH = 3.95 mol·L^{-1}, T = 348.2 K			
1.139	0.0000	3.159×10^{-2}	3.978	0.000	3.229×10^{-2}
1.145	0.0641	1.412×10^{-2}	3.992	0.065	1.439×10^{-2}
1.149	0.1282	9.135×10^{-3}	4.006	0.130	9.320×10^{-3}
1.146	0.1923	7.135×10^{-3}	4.020	0.196	7.332×10^{-3}
1.149	0.2564	5.857×10^{-3}	4.034	0.262	6.029×10^{-3}
1.157	0.3205	5.566×10^{-3}	4.049	0.329	5.719×10^{-3}
1.158	0.3846	5.134×10^{-3}	4.063	0.396	5.294×10^{-3}
1.130	0.4487	4.537×10^{-3}	4.077	0.463	4.816×10^{-3}
1.154	0.5128	4.670×10^{-3}	4.092	0.531	4.879×10^{-3}
1.163	0.5769	4.686×10^{-3}	4.106	0.600	4.885×10^{-3}
1.168	0.6410	4.711×10^{-3}	4.121	0.669	4.914×10^{-3}
1.162	0.7051	4.653×10^{-3}	4.135	0.738	4.901×10^{-3}
1.174	0.8333	4.778×10^{-3}	4.165	0.879	5.031×10^{-3}
NaOH = 6.17 mol·L^{-1}, T = 348.2 K					
1.212	0.0000	4.315×10^{-2}	6.320	0.000	4.485×10^{-2}
1.215	0.1923	1.172×10^{-2}	6.390	0.199	1.228×10^{-2}
1.221	0.3846	7.789×10^{-3}	6.461	0.403	8.240×10^{-3}
1.218	0.6410	6.840×10^{-3}	6.558	0.681	7.397×10^{-3}
1.238	1.0897	8.334×10^{-3}	6.731	1.189	9.178×10^{-3}
1.244	1.2821	9.081×10^{-3}	6.807	1.414	1.011×10^{-2}
1.259	1.6667	1.026×10^{-2}	6.961	1.880	1.163×10^{-2}
NaOH = 7.9 mol·L^{-1}, T = 303.2 K					
1.281	0.0000	5.151×10^{-2}	8.243	0.000	5.382×10^{-2}
1.285	0.1923	1.715×10^{-2}	8.338	0.203	1.805×10^{-2}

dx.doi.org/10.1021/ie301590r | Ind. Eng. Chem. Res. 2012, 51, 15193−15206

Table 4. continued

density, g/mL	$Al(OH)_3$, mol·L^{-1}	SiO_2, mol·L^{-1}	NaOH, mol·kg^{-1}	$Al(OH)_3$, mol·kg^{-1}	SiO_2, mol·kg^{-1}
NaOH = 7.9 mol·L^{-1}, T = 303.2 K					
1.290	0.3846	1.257×10^{-2}	8.435	0.411	1.336×10^{-2}
1.293	0.6410	1.113×10^{-2}	8.567	0.695	1.204×10^{-2}
1.310	1.0897	1.226×10^{-2}	8.805	1.215	1.355×10^{-2}
1.322	1.4103	1.252×10^{-2}	8.980	1.603	1.408×10^{-2}
1.330	1.7949	1.460×10^{-2}	9.196	2.089	1.683×10^{-2}
1.340	2.1795	1.622×10^{-2}	9.419	2.598	1.916×10^{-2}
		NaOH = 7.9 mol·L^{-1}, T = 318.2 K			
1.283	0.0000	5.056×10^{-2}	8.243	0.000	5.275×10^{-2}
1.284	0.1923	1.667×10^{-2}	8.338	0.203	1.756×10^{-2}
1.291	0.3846	1.229×10^{-2}	8.435	0.411	1.305×10^{-2}
1.304	0.6410	1.117×10^{-2}	8.567	0.695	1.198×10^{-2}
1.315	1.0897	1.107×10^{-2}	8.805	1.215	1.220×10^{-2}
1.312	1.4103	1.219×10^{-2}	8.980	1.603	1.382×10^{-2}
1.332	1.7949	1.421×10^{-2}	9.196	2.089	1.635×10^{-2}
1.350	2.1795	1.697×10^{-2}	9.419	2.598	1.990×10^{-2}
1.347	2.4359	1.780×10^{-2}	9.571	2.951	2.135×10^{-2}
1.356	2.6923	2.020×10^{-2}	9.726	3.314	2.460×10^{-2}
1.361	3.0769	2.350×10^{-2}	9.963	3.881	2.945×10^{-2}
		NaOH = 7.9 mol·L^{-1}, T = 333.2 K			
1.277	0.0000	5.149×10^{-2}	8.243	0.000	5.399×10^{-2}
1.279	0.1923	1.647×10^{-2}	8.338	0.203	1.741×10^{-2}
1.276	0.3846	1.165×10^{-2}	8.435	0.411	1.252×10^{-2}
1.295	0.6410	1.014×10^{-2}	8.567	0.695	1.095×10^{-2}
1.303	1.0897	1.091×10^{-2}	8.805	1.215	1.213×10^{-2}
1.316	1.4103	1.298×10^{-2}	8.980	1.603	1.466×10^{-2}
1.319	1.7949	1.418×10^{-2}	9.196	2.089	1.649×10^{-2}
1.339	2.1795	1.587×10^{-2}	9.419	2.598	1.875×10^{-2}
1.351	2.4359	1.761×10^{-2}	9.571	2.951	2.106×10^{-2}
1.345	2.6923	1.865×10^{-2}	9.726	3.314	2.288×10^{-2}
1.367	3.0769	1.923×10^{-2}	9.963	3.881	2.398×10^{-2}
		NaOH = 7.9 mol·L^{-1}, T = 348.2 K			
1.272	0.0000	5.311×10^{-2}	8.243	0.000	5.589×10^{-2}
1.268	0.1923	1.844×10^{-2}	8.338	0.203	1.967×10^{-2}
1.270	0.3846	1.207×10^{-2}	8.435	0.411	1.304×10^{-2}
1.282	0.6410	1.018×10^{-2}	8.567	0.695	1.111×10^{-2}
1.289	1.0897	1.122×10^{-2}	8.805	1.215	1.261×10^{-2}
1.303	1.4103	1.362×10^{-2}	8.980	1.603	1.554×10^{-2}
1.315	1.7949	1.429×10^{-2}	9.196	2.089	1.666×10^{-2}
1.329	2.1795	1.589×10^{-2}	9.419	2.598	1.891×10^{-2}
1.335	2.4359	1.765×10^{-2}	9.571	2.951	2.136×10^{-2}
1.347	2.6923	1.867×10^{-2}	9.726	3.314	2.288×10^{-2}
1.338	3.0769	2.018×10^{-2}	9.963	3.881	2.573×10^{-2}
1.377	3.7179	2.520×10^{-2}	10.478	4.931	3.312×10^{-2}
1.389	3.9744	2.674×10^{-2}	10.654	5.360	3.562×10^{-2}
NaOH = 9.875 mol·L^{-1}, T = 303.2 K					
1.287	0.0000	5.855×10^{-2}	10.574	0.000	6.519×10^{-2}
1.349	0.1923	1.829×10^{-2}	10.704	0.208	1.962×10^{-2}
1.337	0.3846	1.319×10^{-2}	10.836	0.422	1.449×10^{-2}
1.344	0.6410	1.199×10^{-2}	11.016	0.715	1.336×10^{-2}
1.350	0.8333	1.188×10^{-2}	11.154	0.941	1.339×10^{-2}
1.360	1.0897	1.298×10^{-2}	11.342	1.252	1.483×10^{-2}
1.409	2.1795	1.854×10^{-2}	12.196	2.692	2.239×10^{-2}
1.411	3.0769	2.732×10^{-2}	12.970	4.041	3.561×10^{-2}
		NaOH = 9.875 mol·L^{-1}, T = 318.2 K			
1.323	0.0000	5.721×10^{-2}	10.574	0.000	6.195×10^{-2}
1.325	0.1923	1.975×10^{-2}	10.704	0.208	2.158×10^{-2}
1.332	0.3846	1.435×10^{-2}	10.836	0.422	1.582×10^{-2}
1.337	0.6410	1.265×10^{-2}	11.016	0.715	1.418×10^{-2}
1.347	0.8333	1.284×10^{-2}	11.154	0.941	1.450×10^{-2}
1.368	1.0897	1.284×10^{-2}	11.342	1.252	1.457×10^{-2}

dx.doi.org/10.1021/ie301590r | Ind. Eng. Chem. Res. 2012, 51, 15193−15206

Table 4. continued

density, g/mL	$Al(OH)_3$, mol·L^{-1}	SiO_2, mol·L^{-1}	NaOH, mol·kg^{-1}	$Al(OH)_3$, mol·kg^{-1}	SiO_2, mol·kg^{-1}
		NaOH = 9.875 mol·L^{-1}, T = 318.2 K			
1.403	2.1795	2.043×10^{-2}	12.196	2.692	2.477×10^{-2}
1.430	3.0769	2.879×10^{-2}	12.970	4.041	3.704×10^{-2}
1.471	3.9744	3.971×10^{-2}	13.815	5.560	5.385×10^{-2}
1.492	5.2564	5.838×10^{-2}	15.154	8.066	8.800×10^{-2}
		NaOH = 9.875 mol·L^{-1}, T = 333.2 K			
1.333	0.0000	5.871×10^{-2}	10.574	0.000	6.310×10^{-2}
1.316	0.1923	2.153×10^{-2}	10.704	0.208	2.369×10^{-2}
1.334	0.3846	1.501×10^{-2}	10.836	0.422	1.653×10^{-2}
1.337	0.6410	1.311×10^{-2}	11.016	0.715	1.469×10^{-2}
1.346	0.8333	1.300×10^{-2}	11.154	0.941	1.470×10^{-2}
1.359	1.0897	1.452×10^{-2}	11.342	1.252	1.660×10^{-2}
1.386	2.1795	2.128×10^{-2}	12.196	2.692	2.614×10^{-2}
1.409	3.0769	3.193×10^{-2}	12.970	4.041	4.172×10^{-2}
1.441	3.9744	4.539×10^{-2}	13.815	5.560	6.290×10^{-2}
1.410	4.8718	4.776×10^{-2}	14.735	7.269	7.346×10^{-2}
1.497	5.2564	7.093×10^{-2}	15.154	8.066	1.067×10^{-1}
1.480	5.6410	7.821×10^{-2}	15.588	8.904	1.235×10^{-1}
		NaOH = 9.875 mol·L^{-1}, T = 348.2 K			
1.307	0.0000	5.729×10^{-2}	10.574	0.000	6.283×10^{-2}
1.313	0.1923	2.346×10^{-2}	10.704	0.208	2.588×10^{-2}
1.330	0.3846	1.657×10^{-2}	10.836	0.422	1.831×10^{-2}
1.321	0.6410	1.408×10^{-2}	11.016	0.715	1.598×10^{-2}
1.337	0.8333	1.383×10^{-2}	11.154	0.941	1.575×10^{-2}
1.338	1.0897	1.499×10^{-2}	11.342	1.252	1.741×10^{-2}
1.377	2.1795	2.178×10^{-2}	12.196	2.692	2.692×10^{-2}
1.416	3.0769	3.095×10^{-2}	12.970	4.041	4.024×10^{-2}
1.440	3.9744	4.259×10^{-2}	13.815	5.560	5.902×10^{-2}
1.469	5.2564	6.119×10^{-2}	15.154	8.066	9.374×10^{-2}
1.490	5.6410	7.530×10^{-2}	15.588	8.904	1.181×10^{-1}
1.511	6.0256	7.925×10^{-2}	16.037	9.785	1.272×10^{-1}
1.526	6.5385	9.613×10^{-2}	16.659	11.030	1.608×10^{-1}

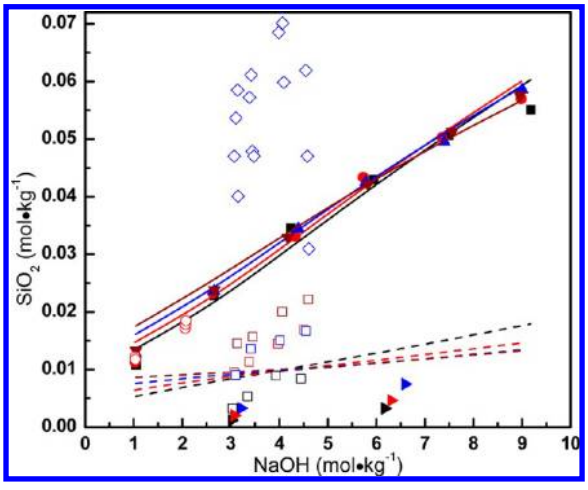

Figure 5. Solubility of sodalite, zeolite A, and amorphous sodium aluminosilicate in NaOH solutions: (solid square) 303.2 K, (solid circle) 318.2 K, (solid up triangle) 333.2 K, (solid down triangle) 348.2 K, (open circle) zeolite A solubility measured by Cizmek et al., (right solid triangel) zeolite A solubility measured by Addai-Mensah et al., (open square) zeolite A solubility measured by Ejaz et al., (open diamond) amorphous sodium aluminosilicate solubility measured by Ejaz et al. The dashed lines represent the estimated solubility using the default databank; the solid lines are the calculated values using regressed parameters.

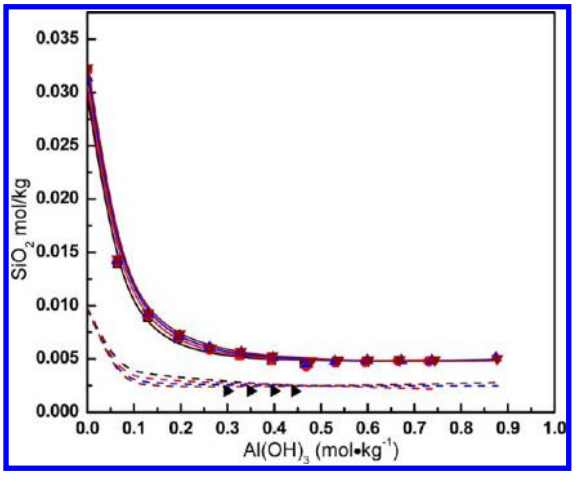

Figure 6. Solubility of sodalite in NaOH−$NaAl(OH)_4$ solutions containing 3.95 mol·L^{-1} NaOH: (solid square) 303.2 K, (solid circle) 318.2 K, (solid up triangle) 333.2 K, (solid down triangle) 348.2 K, (open circle), (solid right triangle) Breurer et al. The dashed lines are the estimated solubility using the default databank; the solid lines represent the calculated values using the regressed parameters.

solubility reported by Ejaz et al. and Addai-Mensah et al. increases with increasing temperature. Similar findings have been reported by Breuer et al.[25] and Barnes et al.[5] on the solubility of sodalite. In the work of Čizmek et al., commercial zeolite A was used, while Ejaz et al. and Addai-Mensah et al. synthesized their zeolite A samples, and their zeolite A compositions are different. This may contribute to the differences in their solubility data. The

dx.doi.org/10.1021/ie301590r | Ind. Eng. Chem. Res. 2012, 51, 15193−15206

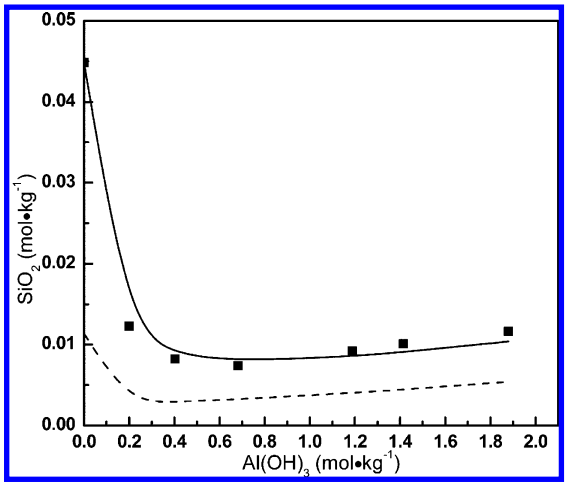

Figure 7. Solubility of sodalite in NaOH−$NaAl(OH)_4$ solutions containing 6.17 mol·L^{-1} NaOH at 348.2 K. The dashed lines represent the estimated solubility using the default databank; the solid lines are the calculated values using the regressed parameters.

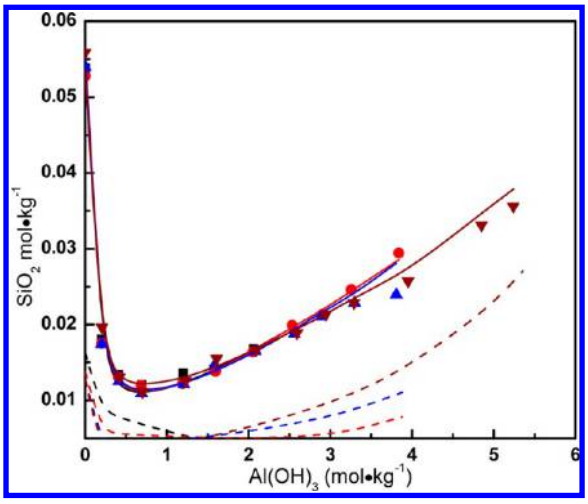

Figure 8. Solubility of sodalite in NaOH−$NaAl(OH)_4$ solutions containing 7.9 mol·L^{-1} NaOH: (solid square) 303.2 K, (solid circle) 318.2 K, (solid up triangle) 333.2 K, (solid down triangle) 348.2 K. The dashed lines represent the estimated solubility using the default databank; the solid lines represent the calculated values using the regressed parameters.

temperature range in the work of Breuer et al. (343.2−523.2 K) and Barnes et al. (363.2−433.2 K) is wider than the present work (303.2−348.2 K) and this may be the reason that they have observed the increasing solubility.

4.3. Evaluation of the Model Parameters. The accuracy of OLI's existing model (available as software package Stream-Analyzer 3.2) in estimating sodalite solubility in NaOH and NaOH−$NaAl(OH)_4$ solutions was evaluated by comparing OLI's prediction to experimental data from the literature and present work. Both sets of data (model predictions and experimental) are plotted in Figures 11 and 12 for the case of gibbsite solubility in NaOH solutions[39] and water activities in Na_2SiO_3 and Na_2SiO_3−NaOH solutions,[40] respectively. As it can be observed, the deviation of OLI predictions from experiments is fairly small which indicates that the parameters are shown to describe the interactions between Na^+−$Al(OH)_4^-$, Na^+−$HSiO_3^-$, Na^+−$H_2SiO_4^{2-}$, OH^-−$Al(OH)_4^-$, OH^-−$HSiO_3^-$ and OH^-−$H_2SiO_4^{2-}$ accurately. However, OLI yielded a relatively large

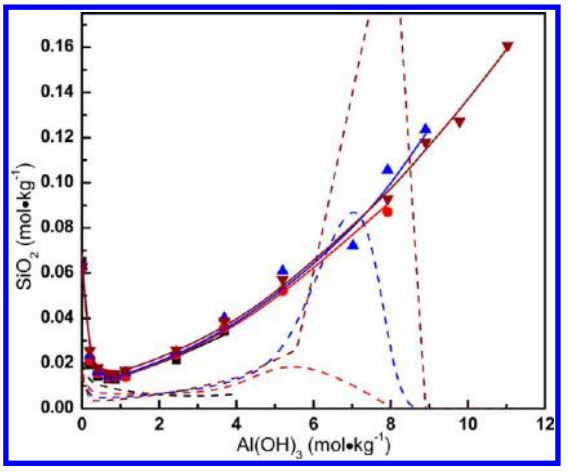

Figure 9. Solubility of sodalite in NaOH−$NaAl(OH)_4$ solutions containing 9.85 mol·L^{-1} NaOH: (solid square) 303.2 K, (solid circle) 318.2 K, (solid up triangle) 333.2 K, (solid down triangle) 348.2 K. The dashed lines represent the estimated solubility using the default databank; the solid lines represent the calculated values using the regressed parameters.

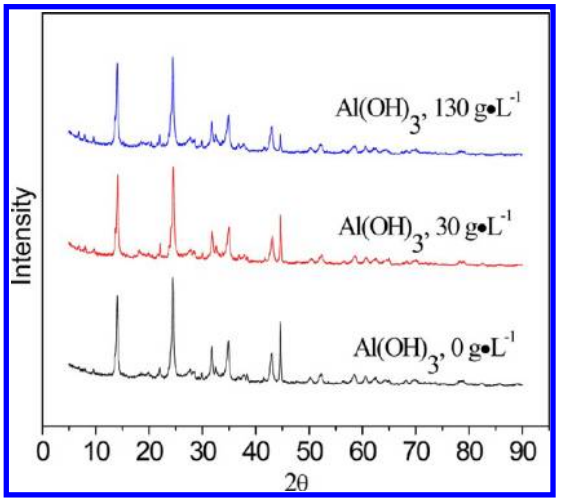

Figure 10. XRD patterns of sodalite after immersion in NaOH−$NaAl(OH)_4$ solutions containing 6.17 mol·L^{-1} NaOH for 48 h at 348.2 K.

deviation when the solubility of sodalite in NaOH and NaOH−$NaAl(OH)_4$ solutions was estimated (see Figures 5−9).

4.4. Model Parameterization. With the purpose of improving the OLI's prediction capability, in regard to sodalite solubility in NaOH and NaOH−$NaAl(OH)_4$ solutions, new model parameters including middle-range interaction parameters for $Al(OH)_4^-$−$HSiO_3^-$, $Al(OH)_4^-$−$H_2SiO_4^{2-}$, $Al(OH)_4^-$−$AlSiO_3(OH)_4^{3-}$, $AlSiO_3(OH)_4^{3-}$−Na^+ and $AlSiO_3(OH)_4^{3-}$−OH^-, together with S^o and Δ_fG^o of sodalite, were obtained via the regression of the experimental solubility data. The regression was done by the OLI's regression program in which the Levenberg−Marquardt algorithm is used. OLI is proprietary software and no standard errors of the parameters were given in the regression results. The model parameters are single-precision floating point numbers. So, seven significant digits are retained as OLI produced. The resulting middle-range interaction parameters are listed in Table 5. S^o and Δ_fG^o of sodalite are found to be 885.5582 J·mol^{-1}·K^{-1} and −13183.294 kJ·mol^{-1}, respectively. The formation enthalpy (Δ_fH^o) of sodalite calculated from S^o and Δ_fG^o is −14098.536 kJ·mol^{-1}. The new Δ_fH^o value agrees very

dx.doi.org/10.1021/ie301590r | Ind. Eng. Chem. Res. 2012, 51, 15193−15206

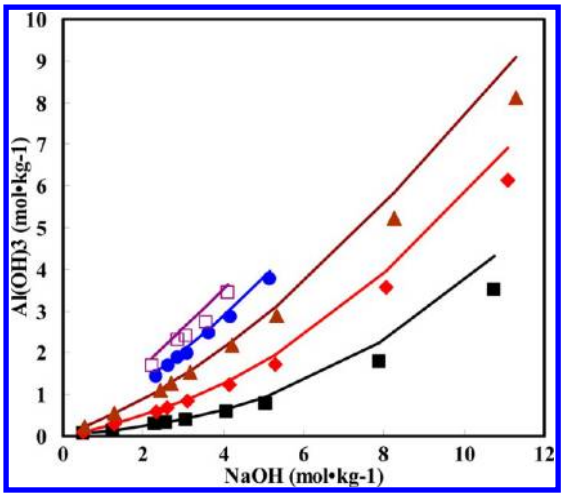

Figure 11. Solubility of gibbsite in NaOH solutions: (■) 313.2 K, (♦) 343.2 K, (▲) 373.2 K, (●) 403.2 K, (□) 443.2 K. The solid lines represent the calculated solubility.

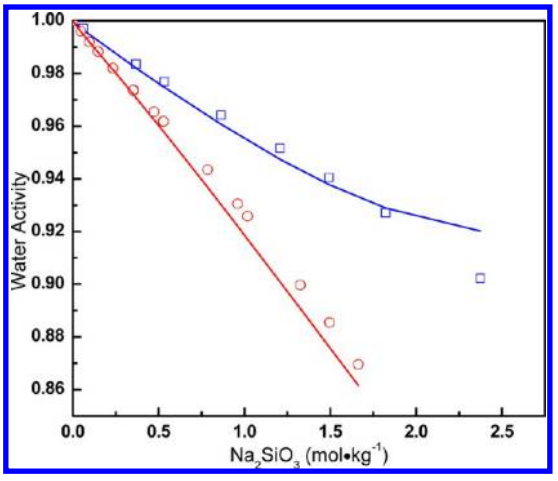

Figure 12. Water activities for the Na_2SiO_3 and Na_2SiO_3–NaOH aqueous solutions at 298.2 K: (□) Na_2SiO_3, (○) Na_2SiO_3–NaOH. The solid lines represent the calculated water activities.

well with the measured $\Delta_f H^\circ$ of the Na_{s-1} sodalite sample by Moloy et al.,[38] which is -14093.2 ± 13.8 kJ·mol^{-1}.

The solubility of sodalite calculated with the newly obtained parameters is displayed in solid lines in Figures 5–9, and the relative deviations between the calculated values using the new model and the experimental solubility are depicted in Figures 13 and 14. The new model results (solid lines in Figure 5) are consistent with the experimental sodium aluminosilicate solubility in pure NaOH solutions with an average relative deviation (AARD) of 7.55%. In the case of NaOH–$NaAl(OH)_4$, the calculated values by the new model (solid lines in Figures 6–9) are in good agreement with experimental data with an AARD of 4.49%.

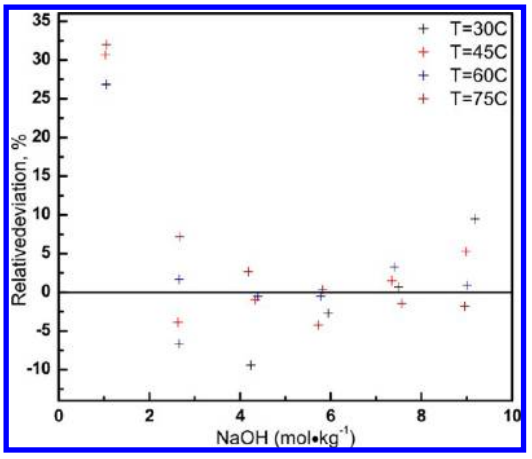

Figure 13. Relative deviation between the calculated and measured solubility in NaOH solutions.

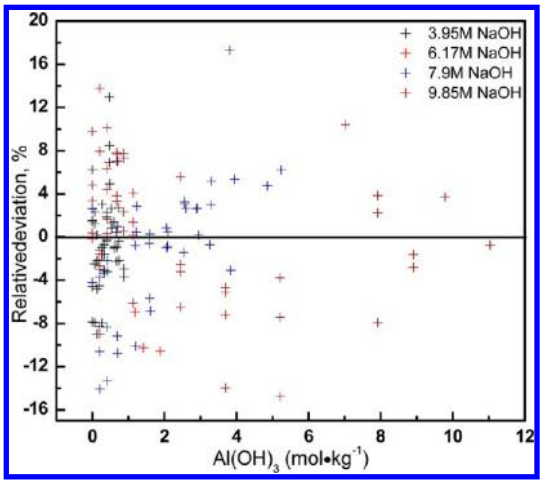

Figure 14. Relative deviation between the calculated and measured solubility in NaOH–$NaAl(OH)_4$ solutions.

Industrial Bayer liquor always contains certain amounts of CO_3^{2-}. CO_3^{2-} may replace OH^- in the sodalite cage and form a less soluble solid. For assessing whether Na_2CO_3 can affect the results, the concentrations of CO_3^{2-} in the NaOH–$NaAl(OH)_4$ filtrate, which was used to determine the solubility of sodalite, were measured by the total organic carbon (TOC) method and retained less than 2.5×10^{-4} mol·L^{-1}. Therefore, the solubility of sodalite in NaOH–$NaAl(OH)_4$ solutions containing 2.5×10^{-4} mol·L^{-1} Na_2CO_3 were predicted by use of the new model parameters regressed above. The AARD (deviation %) was found to be increased by 1.4% compared with the original Na_2CO_3-free results. This error is within the uncertainty of regression. On the basis of the above results, the effect of Na_2CO_3 was not considered in this work.

4.5. Use of the Model. The distribution of silicon species ($HSiO_3^-$, $H_2SiO_4^{2-}$, $AlSiO_3(OH)_4^{3-}$) as a function of temperature

Table 5. MSE Middle Range Interaction Parameters

species *i*	species *j*	BMD0	BMD1	BMD2	CMD0
$Al(OH)_4^-$	$HSiO_3^-$	3649.522	−5.629732	−559864.3	−97.17215
$Al(OH)_4^-$	$H_2SiO_4^{2-}$	178891.7	−295.6676	$-2.7419226 \times 10^{-7}$	165.0333
$Al(OH)_4^-$	$AlSiO_3(OH)_4^{3-}$	1513.133	−21.50032	43285.43	10275.99
$AlSiO3(OH)_4^{3-}$	OH^-	−33.58862	−18.66875	248260.8	10194.96
$AlSiO3(OH)_4^{3-}$	Na^+	−1358.781	21.02259	8639.991	−10408.5

dx.doi.org/10.1021/ie301590r | *Ind. Eng. Chem. Res.* 2012, 51, 15193–15206

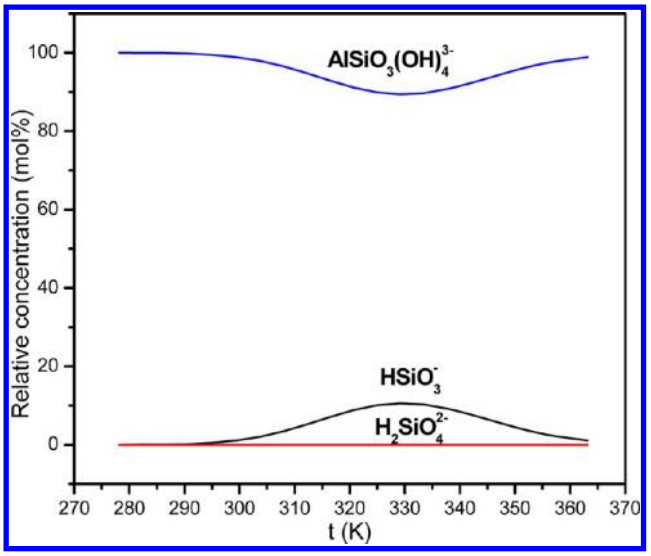

Figure 15. Silicon speciation, as a function of temperature, for sodalite saturated NaOH−$NaAl(OH)_4$ solutions containing 8.011 mol·kg^{-1} NaOH and 4.93 mol·kg^{-1} $Al(OH)_3$.

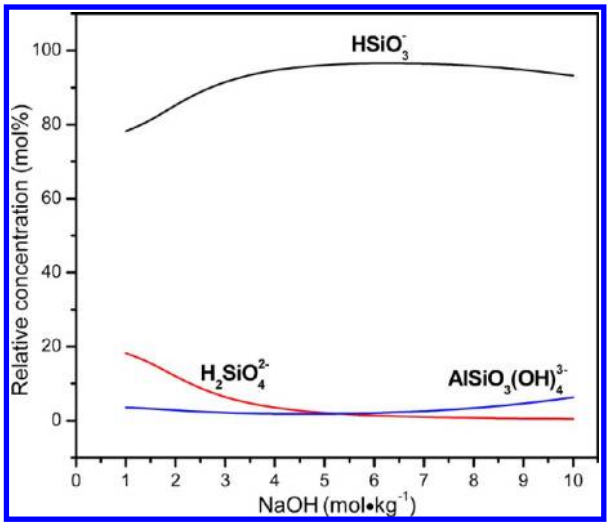

Figure 16. Silicon speciation at 348.2 K, as a function of NaOH concentration, for sodalite saturated NaOH solutions.

and concentrations was calculated by OLI's stream analyzer (version 3.2) with the new parameters. The effect of temperature on the distribution of silicon species is indicated in Figure 15. As can be seen, $AlSiO_3(OH)_4^{3-}$ is the major silicon species in sodalite saturated NaOH−$NaAl(OH)_4$ solutions containing 8.011 mol·kg^{-1} NaOH and 4.93 mol·kg^{-1} $Al(OH)_3$ from 278.2 to 363.2 K, while the maximum relative concentration of $HSiO_3^-$ is 10.58% and the amount of $H_2SiO_4^{2-}$ is very small. Figure 16 shows that the relative concentration of silicon species as a function of NaOH concentration in sodalite saturated pure NaOH solutions at 348.2 K. In this case, $HSiO_3^-$ becomes the most important silicon species. Adding $Al(OH)_3$ to NaOH solution, as shown in Figure 17, results in a sharp decrease of the relative concentration of $HSiO_3^-$, while the relative concentration of $AlSiO_3(OH)_4^{3-}$ has the reverse trend as compared to $HSiO_3^-$.

The solubility of gibbsite, as suggested by Adu-Wusu and Wilcox,[41] is enhanced by a trace amount of silicate in solution. According to the calculated results using the new chemical model, the solubility of gibbsite in 4.293 mol·kg^{-1} NaOH (125 g·L^{-1} Na_2O) at 323.2 K

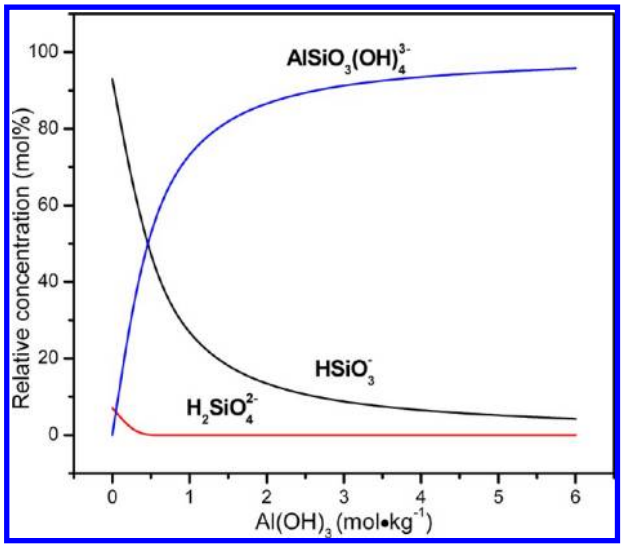

Figure 17. Silicon speciation at 348.2 K, as a function of $Al(OH)_3$ concentration, for sodalite saturated NaOH−$NaAl(OH)_4$ solutions containing 8.011 mol·kg^{-1} NaOH.

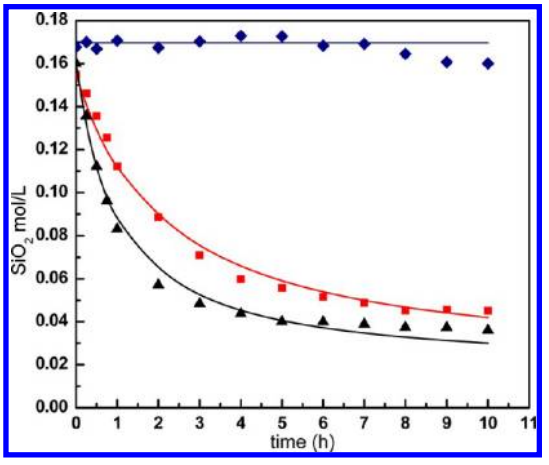

Figure 18. Effect of sodalite dosage on desilication at 343.2 K: (♦) 0 g·L^{-1}, (■) 30 g·L^{-1}, (▲) 60 g·L^{-1}.

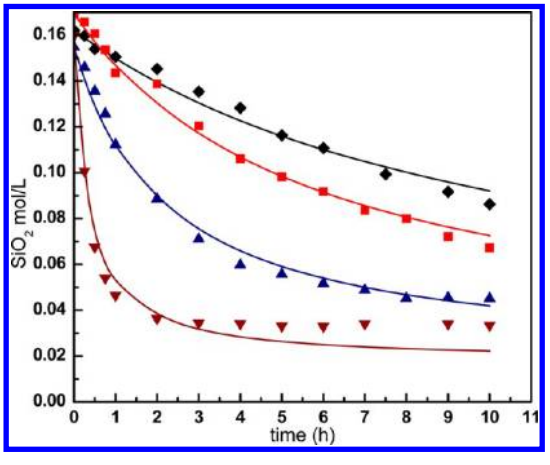

Figure 19. Effect of temperature on desilication: (♦) 323.2 K, (■) 333.2 K, (▲) 343.2 K, (▼) 363.2 K.

increased by 1.7% and 2.5% when adding 0.5 and 0.9 g·L^{-1} SiO_2, respectively. Although the observed values by Adu-Wusu and Wilcox were 3.4% and 5.1% and the predicted values are half of the

dx.doi.org/10.1021/ie301590r | Ind. Eng. Chem. Res. 2012, 51, 15193−15206

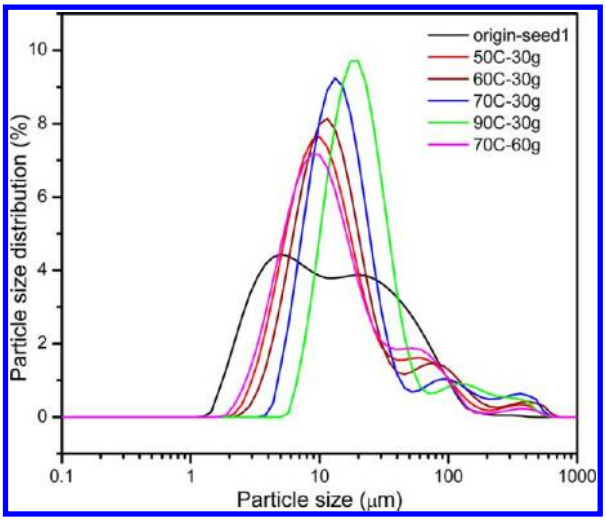

Figure 20. Particle size distributions of the resulting sodalite crystals.

experimental ones, the same trend of the gibbsite solubility increasing with increasing silicate concentration was predicted by the new chemical model.

4.6. Desilication with Sodalite Seeds. Three experiments with different sodalite dosage (no seeds, 30 g·L^{-1}, 60 g·L^{-1}) at 343.2 K have been carried out, and the results are demonstrated in Figure 18. From the experiment results, it can be seen that the SiO_2 concentration was hardly changed in 7 h without sodalite seeds due to the long induction time of sodalite nucleation from clear solution.[42] However, rapid desilication of the NaOH−$NaAl(OH)_4$ solutions occurred when sodalite seeds were added. The SiO_2 concentration dropped to 0.045 and 0.036 mol·L^{-1} after 10 h by seeding with 30 and 60 g·L^{-1} sodalite, respectively. The effect of temperature was further examined at 323.2, 333.2, 343.2, and 363.2 K with fixed 30 g·L^{-1} sodalite seeds, and the results are plotted in Figure 19. As can be seen, the desilication reaction rate was significantly enhanced by increasing temperature. For example, the SiO_2 concentration reached 0.036 mol·L^{-1} after 2 h at 363.2 K indicating that about 80% silica was removed, while the SiO_2 concentration was about 0.086 mol·L^{-1} after 10 h at 323.2 K.

The results of the particle size analysis before and after desilication (Figure 20) showed that the average size after desilication increases with increasing temperature, but decreases with increasing seed dosage. The average particle size of sodalite seed was 8.0 μm, which after desilication at 323.2, 333.2, 343.2, and 363.2 K with 30 g·L^{-1} seed dosage increased to 10.6, 12.1, 14.6, and 19.8 μm, respectively. With no significant fraction of smaller size presented in the product, it is demonstrated that no obvious nucleation occurred and the growth of the seed crystals is the major reason for the desilication.

The kinetics data under different desilication conditions were all fitted using eq 18. The results are shown in Table 6 and Figures 18 and 19. As can be seen, eq 18 is found to be applicable for fitting the kinetics data except a noticeable deviation is observed after 3 h at 363.2 K. The value of k_gA was found to increase with increasing temperature indicating the desilication reaction is endothermic. Because the total surface area had been doubled, the value of k_gA with 60 g·L^{-1} seeds at 343.2 K is about two times larger than that with 30 g·L^{-1} seeds

A single linear relation (R^2 = 0.9973) for $\ln(k_gA)$ versus $\log(1000/T)$ was observed in Figure 21. This implies that a simple Arrhenius relationship can be used to estimate the activation energy for the desilication reaction with sodalite seeds:

Table 6. Model Parameters of the Kinetics of Desilication Reaction

T (K)	dosage (g·L^{-1})	kg × A (h^{-1})
323.2	30	1.167 ± 0.110 × 10^{-2}
333.2	30	2.082 ± 0.149 × 10^{-2}
343.2	30	6.087 ± 0.542 × 10^{-2}
343.2	60	1.328 ± 0.136 × 10^{-1}
363.2	30	3.983 ± 0.914 × 10^{-1}

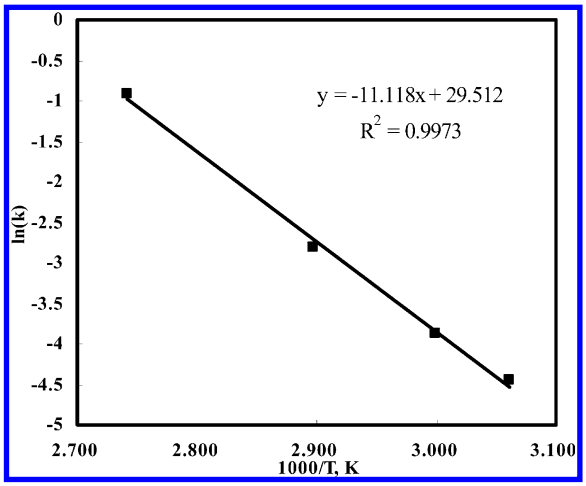

Figure 21. Arrhenius plot for the desilication kinetics.

$$k_gA = k_0A \exp\left(-\frac{E_a}{RT}\right) \quad (19)$$

where k_0 is the pre-exponential factor (h^{-1}·m^{-2}), and E_a (kJ·mol^{-1}) is the activation energy. Regression analysis resulted in an activation energy of 92 ± 14 kJ·mol^{-1} for the desilication reaction. The value of the activation energy obtained in this work is very close to the value of Oku and Yamada,[19] which is 91.1 kJ·mol^{-1}. But it is worth noting that other E_a values have been reported by previous researchers, such as 30 kJ·mol^{-1} by Barnes et al.,[37] and 58.65 kJ·mol^{-1} by Ma et al.[11] Finally, the overall rate equation for the desilication with sodalite seeds may be written as

$$-\frac{d\sigma}{dt} = \exp(29.512 - 11118/T)(\sigma)^2 \quad (20)$$

The above results suggest that the desilication reaction rate can be accelerated by adding more seeds or increasing the temperature. After 2 h desilication with sodalite seed at 363.2 K, 80% silica was removed from the NaOH−$NaAl(OH)_4$ solution but the SiO_2 concentration was still greater than the acceptable level in most alumina refineries. Therefore, a desilication agent such as CaO is still required for a smaller SiO_2 concentration.

5. CONCLUSIONS

Both NaOH and $Al(OH)_3$ were found to have a strong effect on the solubility of sodalite, while the effect of temperature on the solubility was very limited. A MSE-based chemical model for prediction of the solubility of sodalite was developed. New midrange interaction parameters for $Al(OH)_4^-$−$HSiO_3^-$, $Al(OH)_4^-$−$H_2SiO_4^{2-}$, $Al(OH)_4^-$−$AlSiO_3(OH)_4^{3-}$, $AlSiO_3(OH)_4^{3-}$−Na^+ and $AlSiO_3(OH)_4^{3-}$−OH^-, together with S^o (885.5582 J·mol^{-1}·K^{-1})

dx.doi.org/10.1021/ie301590r | Ind. Eng. Chem. Res. 2012, 51, 15193−15206

and $\Delta_f G^\circ(-13183.294\ \mathrm{kJ\cdot mol^{-1}})$ of sodalite, were obtained via regression of the solubility data. The calculations using the new chemical model agreed well with the experimental solubility.

Silicon species distribution was analyzed with the aid of the new model. It was found that $HSiO_3^-$ is the major silicon species in pure NaOH solutions, whereas $AlSiO_3(OH)_4^{3-}$ is the most important species in aluminate-rich NaOH−$NaAl(OH)_4$ solutions. In addition, increasing gibbsite solubility by the addition of silicate was partly predicted by the new model.

The desilication reaction rate was found to increase with greater temperature or more seeds. Under the optimal conditions, 80% silica was removed from the NaOH−$NaAl(OH)_4$ solution. A second order kinetic model was proposed, giving an activation energy of $92 \pm 14\ \mathrm{kJ\cdot mol^{-1}}$ over the temperature range 323.2−363.2 K.

AUTHOR INFORMATION

Corresponding Author

*Tel.: +86-10-62551557. Fax: +86-10-62551557. E-mail: zhibaoli@home.ipe.ac.cn.

Notes

The authors declare no competing financial interest.

ACKNOWLEDGMENTS

The support of the National Natural Science Foundation of China (Grant No. 21076212 and No. 21146006) is gratefully acknowledged.

REFERENCES

(1) Misra, C. *Industrial Alumina Chemicals; ACS Monograph*; American Chemical Society: Washington, DC, 1986.

(2) Croker, D.; Loan, M.; Hodnett, B. K. Desilication Reactions at Digestion Conditions: An in Situ X-ray Diffraction Study. *Cryst. Growth Des.* **2008**, *8*, 4499−4505.

(3) Ho, G. E.; Robertson, W. A.; Roach, G. I. D.; Antonovsky, A. Morphological Study of Bayer Process Desilication Product and Its Application to Laboratory and Plant Digests. *Ind. Eng. Chem. Res.* **1992**, *31*, 982−986.

(4) Zheng, K. L.; Gerson, A. R.; Addai-Mensah, J.; Smart, R. S. C. The Influence of Sodium Carbonate on Sodium Aluminosilicate Crystallisation and Solubility in Sodium Aluminate Solutions. *J. Cryst. Growth* **1997**, *171*, 197−208.

(5) Barnes, M. C.; Addai-Mensah, J.; Gerson, A. R. The Solubility of Sodalite and Cancrinite in Synthetic Spent Bayer Liquor. *Colloids Surf., A* **1999**, *157*, 101−116.

(6) Papanastassiou, D.; Csoke, B.; Solymár, K. Improved Preparation of the Greek Diasporic Bauxite for Bayer-Process. In *Light Metals*; Schneider, W., Ed.; The Minerals, Metals and Materials Society (TMS): Warrendale, PA, 2002; pp 67−74.

(7) Xu, Z. H.; Plitt, V.; Liu, Q. Recent Advances in Reverse Flotation of Diasporic Ores—A Chinese Experience. *Miner. Eng.* **2004**, *17*, 1007−1015.

(8) Huang, C. B.; Wang, Y. H. Removal of Aluminosilicates from Diasporic-Bauxite by Selective Flocculation Using Sodium Polyacrylate. *Sep. Purif. Technol.* **2008**, *59*, 299−303.

(9) Smith, P. The Processing of High Silica Bauxites—Review of Existing and Potential Processes. *Hydrometallurgy* **2009**, *98*, 162−176.

(10) Hollitt, M. J.; Crisp, A. J.; Staker, W. S.; Roe, G. M.; Rodda, D. P. Process for Removing Reactive Silica from a Bayer Process Feedstock. U.S. Patent 6,309,615, October 30, 2001.

(11) Ma, J. Y.; Li, Z. B.; Xiao, Q. G. A New Process for Al_2O_3 Production from Low-Grade Diasporic Bauxite Based on Reactive Silica Dissolution and Stabilization in NaOH−$NaAl(OH)_4$ Media. *AIChE J.* **2012**, *58*, 2180−2191.

(12) Whittington, B. I. The Chemistry of CaO and $Ca(OH)_2$ Relating to the Bayer Process. *Hydrometallurgy* **1996**, *43*, 13.

(13) Forte, G.; Dufour, R. Process for the Removal of Silica from an Alkaline Solution Containing Sodium Aluminate. U.S. Patent 6,086,834, June 11, 2000.

(14) Agency, F. S. Food Standards Agency—Current EU approved additives and their E Numbers. http://www.food.gov.uk/safereating/additivesbranch/enumberlist (accessed Jun 1, 2012).

(15) Jolivet, J.-P.; Chanéac, C.; Chiche, D.; Cassaignon, S.; Durupthy, O.; Hernandez, J. Basic Concepts of the Crystallization from Aqueous Solutions: The Example of Aluminum Oxy(hydroxi)des and Aluminosilicates. *C.R. Geosci.* **2011**, *343*, 113−122.

(16) Gerson, A. R.; Zheng, K. L. Bayer Process Plant Scale: Transformation of Sodalite to Cancrinite. *J. Cryst. Growth* **1997**, *171*, 209−218.

(17) Ejaz, T.; Jones, A. G.; Graham, P. Solubility of Zeolite A and Its Amorphous Precursor Under Synthesis Conditions. *J. Chem. Eng. Data* **1999**, *44*, 574−576.

(18) Addai-Mensah, J.; Li, J.; Rosencrance, S.; Wilmarth, W. Solubility of Amorphous Sodium Aluminosilicate and Zeolite A Crystals in Caustic and Nitrate/Nitrite-Rich Caustic Aluminate Liquors. *J. Chem. Eng. Data* **2004**, *49*, 1682−1687.

(19) Oku, T.; Yamada, K. The Dissolution Rate of Quartz and the Rate of Desilication in the Bayer Liquor. In *Light Metals*; Nuttal, K., Ed.; The Minerals, Metals & Materials Society (TMS): Warrendale, PA, 1971; pp 9−14.

(20) Čimek, A.; Komunjer, L.; Subotić, B.; Široki, M.; Rončević, S. Kinetics of Zeolite Dissolution: Part 1. Dissolution of Zeolite A in Hot Sodium Hydroxide. *Zeolites* **1991**, *11*, 258−264.

(21) Gasteiger, H. A.; Frederick, W. J.; Streisel, R. C. Solubility of Aluminosilicates in Alkaline Solutions and a Thermodynamic Equilibrium Model. *Ind. Eng. Chem. Res.* **1992**, *31*, 1183−1190.

(22) Park, H.; Englezos, P. Thermodynamic Modeling of Sodium Aluminosilicate Formation in Aqueous Alkaline Solutions. *Ind. Eng. Chem. Res.* **1999**, *38*, 4959−4965.

(23) Gout, R.; Pokrovski, G. S.; Schott, J.; Zwick, A. Raman Spectroscopic Study of Aluminum Silicate Complexes at 20 °C in Basic Solutions. *J. Solution Chem.* **2000**, *29*, 1173−1186.

(24) Hefter, G. T.; Tomkins, R. P. T. *The Experimental Determination of Solubilities*; 1st ed.; John Wiley & Sons: Chichester, UK, 2003.

(25) Breuer, R. G.; Barsotti, L. R.; Kelly, A. C. Behavior of Silica in Sodium Aluminate Solutions. In *Extractive Metallurgy of Aluminium*; Gerard, G., Stroup, P. T., Eds.; Interscience Publishers: New York, 1963; Vol. *1*, pp 133−158.

(26) Lippincott, E. R.; Psellos, J. A.; Tobin, M. C. The Raman Spectra and Structures of Aluminate and Zincate Ions. *J. Chem. Phys.* **1952**, *20*, 536−536.

(27) Moolenaar, R. J.; Evans, J. C.; McKeever, L. D. Structure of the Aluminate Ion in Solutions at High pH. *J. Chem. Phys.* **1970**, *74*, 3629−3636.

(28) Barcza, L.; Pálfalvi-Rózsahegyi, M. The Aluminate Lye as a System of Equilibria. *Mater. Chem. Phys.* **1989**, *21*, 345−356.

(29) Iler, R. K. *The Chemistry of Silica: Solubility, Polymerization, Colloid and Surface Properties and Biochemistry of Silica*; John Wiley & Sons: Chichester, UK, 1979.

(30) Provis, J. L.; Duxson, P.; Lukey, G. C.; Separovic, F.; Kriven, W. M.; van Deventer, J. S. J. Modeling Speciation in Highly Concentrated Alkaline Silicate Solutions. *Ind. Eng. Chem. Res.* **2005**, *44*, 8899−8908.

(31) Wang, P. M.; Anderko, A.; Young, R. D. A Speciation-Based Model for Mixed-Solvent Electrolyte Systems. *Fluid Phase Equilib.* **2002**, *203*, 141−176.

(32) Azimi, G.; Papangelakis, V. G.; Dutrizac, J. E. Modelling of Calcium Sulphate Solubility in Concentrated Multicomponent Sulphate Solutions. *Fluid Phase Equilib.* **2007**, *260*, 300−315.

(33) Azimi, G.; Papangelakis, V. G. Thermodynamic Modeling and Experimental Measurement of Calcium Sulfate in Complex Aqueous Solutions. *Fluid Phase Equilib.* **2010**, *290*, 88−94.

(34) OLI Aqueous Electrolytes—Process Chemistry, Inorganic and Organic, MSE and AQ models. http://www.olisystems.com/ (accessed Jun 2, 2012).

(35) Tanger, J. C.; Helgeson, H. C. Calculation of the Thermodynamic and Transport Properties of Aqueous Species at High Pressures and Temperatures; Revised Equations of State for the Standard Partial Molal Properties of Ions and Electrolytes. *Am. J. Sci.* **1988**, *288*, 19−98.
(36) Jia, Y. F.; Demopoulos, G. P. Coprecipitation of Arsenate with Iron(III) in Aqueous Sulfate Media: Effect of Time, Lime as Base and Co-Ions on Arsenic Retention. *Water Res.* **2008**, *42*, 661−668.
(37) Barnes, M. C.; Addai-Mensah, J.; Gerson, A. R. The Kinetics of Desilication of Synthetic Spent Bayer Liquor and Sodalite Crystal Growth. *Colloids Surf., A* **1999**, *147*, 283−295.
(38) Moloy, E. C.; Liu, Q. Y.; Navrotsky, A. Formation and Hydration Enthalpies of the Hydrosodalite Family of Materials. *Microporous Mesoporous Mater.* **2006**, *88*, 283−292.
(39) Russell, A. S.; Edwards, J. D.; Taylor, C. S. Solubility and Density of Hydrated Aluminas in NaOH Solutions. *J. Met.* **1955**, 1123−1128.
(40) Park, H.; Englezos, P. Osmotic Coefficient Data for Na_2SiO_3 and Na_2SiO_3−NaOH by an Isopiestic Method and Modeling Using Pitzer's Model. *Fluid Phase Equilib.* **1998**, *153*, 87−104.
(41) Adu-Wusu, K.; Wilcox, W. R. Kinetics of Silicate Reaction with Gibbsite. *J. Colloid Interface Sci.* **1991**, *143*, 127−138.
(42) Zhang, Y. F.; Li, Y. H.; Zhang, Y. Supersolubility and Induction of Aluminosilicate Nucleation from Clear Solution. *J. Cryst. Growth* **2003**, *254*, 156−163.